nature food

Article

https://doi.org/10.1038/s43016-024-01082-y

# Multiplexed food-borne pathogen detection using an argonaute-mediated digital sensor based on a magnetic-bead-assisted imaging transcoding system

Received: 7 September 2023

Accepted: 31 October 2024

Published online: 2 January 2025

Check for updates

Zhipan Wang [1,4], Xinrui Cheng [1,4], Aimin Ma [1], Feng Jiang [2] & Yiping Chen [1,3]

Accurate, sensitive and multiplexed detection of food-borne pathogens is crucial for assessing food safety risks. Here we present a digital DNA-amplification-free nucleic acid detection assay to achieve multiplexed and ultrasensitive detection of three food-borne pathogens. We used mesophilic *Clostridium butyricum* argonaute and magnetic beads in a digital carrier system (d-MAGIC). *Clostridium butyricum* argonaute, with its two-guide accurate cleavage activity, precisely targets and cleaves fluorescence-quencher reporters corresponding to different bacteria through a two-step process. The system uses fluorescence-encoded magnetic beads as programmable multi-probes, allowing the simultaneous detection of multiple pathogens and easy data interpretation via artificial intelligence. The method showed a wide detection range ($10^1$ to $10^7$ CFU ml$^{-1}$) and a low limit of detection of 6 CFU ml$^{-1}$ for food-borne pathogens without DNA amplification. Digital nucleic acid testing using d-MAGIC can become a next-generation strategy for accurate and convenient pathogen detection.

Food-borne diseases are responsible for 600 million illnesses and 420,000 deaths each year. The World Health Organization has identified food-borne pathogens as the primary cause of these diseases[1]. These pathogens can easily spread in various environments and food samples, leading to serious health issues such as recurrent intestinal inflammation, diarrhoea, vomiting, chronic kidney diseases and even death[2,3]. To prevent and control outbreaks of food-borne diseases, it is crucial to have sensitive, rapid and multiplexed methods for detecting food-borne pathogens. Although microbial culture[4] procedures provide reliable results, they are time consuming. Immunoassays[5] are rapid but insensitive, and they require expensive antibodies. Polymerase chain reaction (PCR)[6] and real-time quantitative PCR (qPCR)[7] are considered the gold standards owing to their high sensitivity and accuracy in detecting food-borne pathogens. However, the DNA amplification step is susceptible to contamination from ambient aerosols[8–11]. In recent years, digital biosensors with single-molecule sensitivity have gained popularity for nucleic acid detection. Among these, the clustered regularly interspaced short palindromic repeats associated proteins (CRISPR–Cas)-mediated digital droplet PCR (ddPCR) strategy[12–15] has shown promise for genome-editing tests with ultra-sensitivity, accuracy and reproducibility. However, its ability to simultaneously detect multiple targets is limited owing to the unspecific trans-cleavage of the CRISPR–Cas enzyme. In addition, the production of droplets in ddPCR often requires complex microfluidic chips, making it necessary to use sophisticated equipment[16,17].

[1]College of Food Science and Technology, Huazhong Agricultural University, Wuhan, China. [2]Key Laboratory of Detection Technology of Focus Chemical Hazards in Animal-Derived Food for State Market Regulation, Wuhan, China. [3]State Key Laboratory of Marine Food Processing and Safety Control, Dalian Polytechnic University, Dalian, China. [4]These authors contributed equally: Zhipan Wang, Xinrui Cheng. e-mail: chenyiping@mail.hzau.edu.cn

Some researchers have recently combined fluorescence signals in non-uniform droplets with artificial intelligence (AI) recognition technology to overcome these drawbacks[18]. However, further improvements are still needed to enhance the stability and accuracy of this approach. Consequently, there is a need to explore a powerful nucleic acid-guided endonuclease to achieve sensitive and multiplexed detection. In addition, a carrier that can replace droplets as a signal probe is required to simplify the analytical process of digital detection.

Argonautes (Agos) are endonucleases guided by nucleic acids that can be activated by specific nucleic acid molecules. They show excellent specificity in their endonuclease activity[19,20], making them a promising alternative to the CRISPR–Cas system for programmable and multiplexed nucleic acid detection. Agos, such as *Pyrococcus furiosus*[21–23] and *Thermus thermophilus*[24,25], which are hyperthermophilic, have been used as tools for specific DNA sequence cleavage in biosensors, enabling the multiplexed detection of tumour and pathogen biomarkers. However, these approaches still require the integration of PCR in a two-step process, involving cumbersome tools, high temperatures and DNA amplification. On the other hand, *Clostridium butyricum* argonautes (CbAgo), as prokaryotic Agos, can perform simultaneous endonucleolytic cleavage of complementary DNA in vitro at room temperature[26,27], using small 5′-phosphorylated DNA guides. CbAgo can cleave targets of single- and double-stranded DNA substrates at specific locations, precisely the 10th and 11th nucleotide from the 5′ end of the guide DNA (gDNA). Furthermore, the short DNA chain generated by CbAgo cleavage can serve as a secondary guide for further specific target cleavage[20,28,29]. The endonuclease activity and two-step cleavage reaction of CbAgo makes it a potentially valuable tool for accurate and multiplexed detection of food-borne pathogen DNA in vitro.

Magnetic beads (MBs) are crucial nanomaterials with various applications in in vivo imaging, in vitro diagnosis and food safety, thanks to their distinctive properties such as superparamagnetic behaviour, therapeutic effectiveness, low toxicity, site-specific targeting and controllable magnetic field[30–32]. Consequently, MBs have emerged as promising candidate carriers for digital detection, replacing droplets. Furthermore, the implementation of tyramine (TA) signal amplification (TSA) based on traditional enzymatic amplification[33,34] theories can enhance the binding efficiency of fluorescent molecules to the surfaces of MBs. However, magnetic aggregation presents a challenge in the application of MBs. Fortunately, AI has proven to possess exceptional recognition capabilities[32,35], particularly in areas such as image processing and intelligent identification. Therefore, AI can be applied to sort and predict the results generated by multiplexed biosensors, as well as to enhance sensitivity[36]. AI-assisted recognition technology has already been successful in decoding cell-type specificity and predicting downstream pathways[37,38], as well as determining non-coding variant effects for various aspects of regulatory proteins[39], all of which are highly complex. Hence, AI-based methods have the potential to overcome[18] the limitations of conventional approaches and can be used to decode the fluorescent MBs utilized in multiplexed digital detection in biosensors.

In this study, we presented a mesophilic CbAgo-assisted digital nucleic acid detection platform (d-MAGIC), which could achieve digital, multiplexed nucleic acid detection of three food-borne pathogens simultaneously. To enable digital detection, we use MBs to create MB–TA–streptavidin (SA) conjugates. The MBs are impregnated with TA and then conjugated with SA to serve as a precursor for fluorescence encoding. This encoding is used for digital detection. Specifically, the MB–TA–SA conjugates bind biotin–fluorescence-quencher (FQ) reporters to prepare programmable fluorescent-encoding MBs. Through different coding states of the encoded MBs in fluorescence images, we develop an AI algorithm platform named 'Panda'. This platform accurately classifies, grades and counts MBs. It also calculates the nucleic acid concentration based on the total number of obtained fluorescent MBs.

Our programmable detection platform represents a significant advancement in single and multiplexed food-borne pathogen detection. It shows high sensitivity to $10^1$ colony-forming units (CFU) $ml^{-1}$ without DNA amplification. The d-MAGIC platform introduces three key innovations. (1) By integrating programmable CbAgo and MBs with AI-assisted decoding, we achieve digital, amplification-free and ultrasensitive detection of three food-borne pathogens simultaneously. (2) The use of micrometre MBs as digitization and encoding carriers simplifies traditional droplet digitization methods and provides resistance to interference owing to their superparamagnetism. (3) The d-MAGIC platform has shown the critical role of developing AI-based image recognition in optimizing detection systems. By creating an algorithm for curve recognition, we enabled efficient decoding and quantitative signal analysis. The integration of uniform-sized MBs with an in situ tyramine affinity system provides numerous robust binding sites, with the uniformity of the MBs ensuring precise outcomes, thereby significantly reducing reliance on conventional DNA amplification techniques. In summary, this study develops a CbAgo-assisted digital and multiplexed nucleic acid detection technology. It is based on a programmable MB-assisted imaging transcoding system and AI algorithm for identifying food-borne pathogen DNA.

## Results

### Method overview

In this method, two different specific gDNAs were designed for each food-borne pathogen, *Salmonella enterica* subsp. *enterica* serovar Typhimurium, *Staphylococcus aureus* and *Listeria monocytogenes* (Fig. 1a). The gDNAs were modified with 5′-phosphorylation. During the test, the gDNAs loaded into CbAgos could hybridize with the DNA of the food-borne pathogens. The CbAgos could then specifically cleave the target DNA at specific sites, allowing the target DNA to be precisely cleaved to a small segment as the secondary gDNA. The secondary gDNA can bind specifically to the CbAgo in the system, forming new CbAgo–gDNA conjugates that can associate with FQ reporters. The FQ reporters have a fluorescent end modified with biotin and can be cleaved by CbAgo because they are specifically paired with the secondary gDNAs.

In this study, homogeneous MBs were used as encoding beads to replace monodisperse droplets in standard digital nucleic acid assays for AI-decoding digital counting. The pre-encoded MB–TA–SA conjugates were constructed from carboxyl acid-modified MBs. Tyramine was decorated on the MBs, followed by the covalent binding of streptavidin to prepare the MB–TA–SA conjugates (Fig. 1b). The three different fluorescent signals coupling with the biotin with a fluorescent moiety were specifically encoded to the surface of MB–TA–SA conjugates for digital readout via the interaction between streptavidin and biotin (Fig. 1b). The substrates were then removed by magnetic separation, and fluorescence images of the encoding MBs were observed and captured using confocal laser scanning microscopy (CLSM). These images were then converted to greyscale images for decoding using AI (Fig. 1c). The quantitative association between the encoding MBs and the target DNA can be established by AI decoding, enabling digital and multiplexed detection of *S.* Typhimurium, *S. aureus* and *L. monocytogenes* without DNA amplification (Fig. 1c).

### Characterization of CbAgo

The CbAgo used in the experiments, which shows two-step cleavage activity, was prepared in our laboratory. This two-step cleavage mechanism is achieved by using the short DNA fragments generated during the primary cleavage as new guides, which bind to CbAgo for further specific cleavage reactions[18,23,25] (Fig. 2a). The secondary cleavage reaction is believed to enhance the immunity against foreign DNA in prokaryotic Agos, and this property has been previously confirmed in our study and other studies[40,41]. To begin, we used matrix-assisted laser desorption and ionization–time of flight (MALDI–TOF/TOF) to determine

https://doi.org/10.1038/s43016-024-01082-y

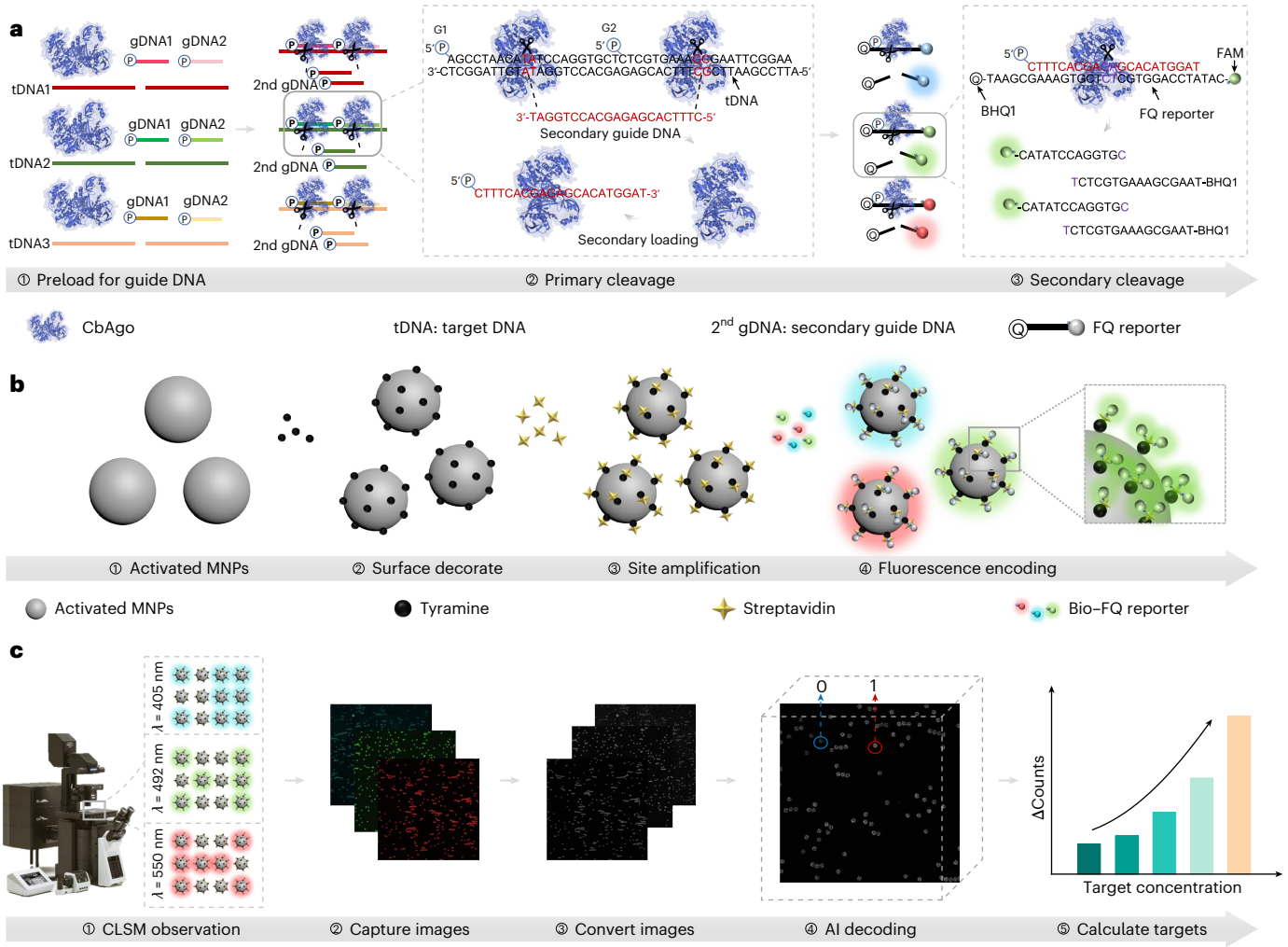


**Fig. 1 | Scheme of the Ago-protein-mediated digital nucleic acid biosensor based on a programmable MB-assisted imaging transcoding system. a**, Principle of the CbAgo-mediated two-step accurate cleavage reaction (Protein Data Bank (PDB) code 6QZK). **b**, Synthesis of MB–TA–SA conjugates and combination with FQ reporters to achieve fluorescence encoding. **c**, Schematic of fluorescence encoding imaging and AI-mediated decoding of MB conjugate counting.

the molecular weight of CbAgo, which was found to be approximately 87.83 kDa (Fig. 2b). This result was consistent with the findings from gel electrophoresis (Fig. 2c). Furthermore, the secondary structure of CbAgo was characterized using circular dichroism spectroscopy. The spectroscopy revealed an absorbance peak ranging from 200 nm to 240 nm (Fig. 2d) and the percentage composition of α-helix at 18.3%, β-sheet at 23.3%, β-turn at 22.6% and random coil at 35.8% (Fig. 2e).

## Characterization of MB–TA–SA conjugates

To confirm the conjugation process, the MB–TA–SA conjugates were characterized using scanning electron microscopy (SEM) and a nanoparticle size potential analyser. SEM images (Fig. 2f and Supplementary Fig. 4a,b) revealed that the surface of the MBs became rough and small particles appeared when TA–SA was modified. Elemental analysis (C, N, O, P, S and Fe) was also performed to verify this conclusion (Fig. 2g and Supplementary Fig. 4c). The MB–TA–SA conjugates showed minimal changes in elemental content compared with the MBs, with a decrease in C and Fe content and an increase in the other four elements. This suggested that streptavidin was successfully attached to the surface of the MBs via tyramine (Fig. 2h). The zeta potential and particle size analysis yielded similar results as SEM and elemental analysis (Fig. 2i). The presence of streptavidin on the MB surface was confirmed by the increase in zeta potential from −11.53 mV to −8.37 mV because tyramine has a neutral charge and streptavidin has a positive charge at neutral pH. In addition, the particle size diameters of the MBs increased after the bioconjugation with streptavidin through the tyramine system (Fig. 2j). All these characterization experiments provided evidence for the presence of streptavidin on the MB surface tyramine via conjugation. In addition, an MB–SA conjugate was prepared in which streptavidin was directly conjugated to the surface of the MBs without the tyramine system. The modification amount of streptavidin was found to be three times higher when using the tyramine system (Fig. 2k), indicating the effectiveness of the tyramine system in enhancing streptavidin binding on the MB surface.

## Programmable MB-assisted imaging transcoding system

To achieve programmable encoding of MBs, fluorescence reporters based on the biotin–SA interaction were used. MB–TA–SA conjugates (3 μm) were chosen as the coding carrier to bind fluorescent probes with biotin at the 5′-end (bio–FQ reporters). This was accomplished through secondary cleavage of CbAgo, resulting in a fluorescent MB encoding system. The encoding process involved the formation of complexes between MB–TA–SA–bio–FQ reporters through the coupling reaction between biotin and streptavidin. Importantly, different fluorescent probes could bind to the same or different MB–TA–SA microspheres without affecting image acquisition or AI decoding. Successfully

https://doi.org/10.1038/s43016-024-01082-y

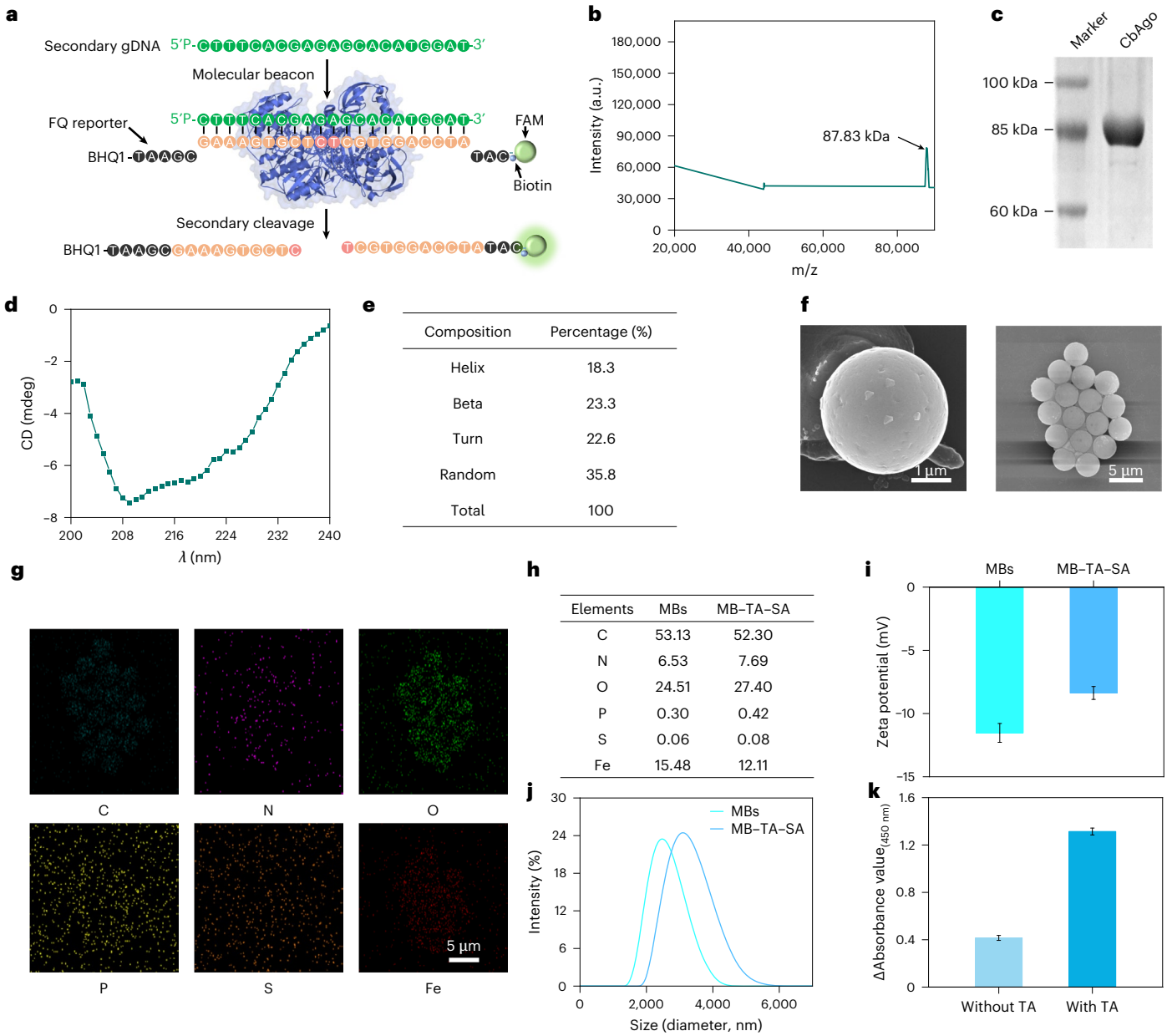


**Fig. 2 | Characterization of CbAgo and MB–TA–SA conjugates. a**, Secondary cleavage principle of CbAgo (*L. monocytogenes* was used as an example, PDB code 6QZK). **b**, MALDI–TOF/TOF map of CbAgo. **c**, Gel electropherogram of CbAgo ($n = 3$). **d**, Circular dichroism chromatogram of CbAgo. **e**, Secondary structure of CbAgo. **f**, Characterization of single MB–TA–SA (left) and MB–TA–SA conjugates (right) by SEM ($n = 3$). **g**, Elemental analysis of the MB–TA–SA conjugates ($n = 3$). The scale bar applies to all images in **g**. **h**, Elemental comparison between MBs and MB–TA–SA conjugates. **i**, Zeta potential comparison of MBs and MB–TA–SA conjugates (data are presented as means ± s.d., $n = 3$). **j**, Change in particle sizes before (left) and after surface modification (right) ($n = 3$). **k**, Signal comparison of MBs modified without and with tyramine (data are presented as means ± s.d., $n = 3$).

encoded MB–TA–SA microspheres by different FQ reporters showed different coding information at various excitation wavelengths (Fig. 3a).

The AI decoding process was conducted using a self-constructed software called PandaCounting.exe (Panda) in our laboratory (Fig. 3a). In this process, the captured images were initially classified based on the colour of the fluorescence reporters (blue, red and green). The images were then grouped into separate files, with blue images representing *S.* Typhimurium, red images representing *S. aureus* and green images representing *L. monocytogenes*.

These sorted images were converted into greyscale and binarized to eliminate background interferences. To determine whether the MB–TA–SA–bio–FQ reporter conjugates were successfully encoded, the fluorescence intensity in the images needed to exceed a certain threshold. If it did, the image would be recognized as '1' for counting purposes; otherwise, it would be recognized as '0' and not counted. When conducting the counts, only MBs in images with an aspect ratio greater than 0.7 were taken into account. However, it was observed that the high energy of the confocal laser could cause the MBs to form magnetic chains, potentially impacting count accuracy. To overcome this issue, the Panda algorithm included a graph-splitting function. This function used the aspect ratio value and split the image when the aspect ratio was too large. In addition, aggregated MBs were identified and segmented when their aspect ratio exceeded 2.

To evaluate the accuracy of Panda, the results were compared with those of manual counting and commercial software (ImageJ). The findings aligned with our expectations. The numbers of MBs counted

https://doi.org/10.1038/s43016-024-01082-y

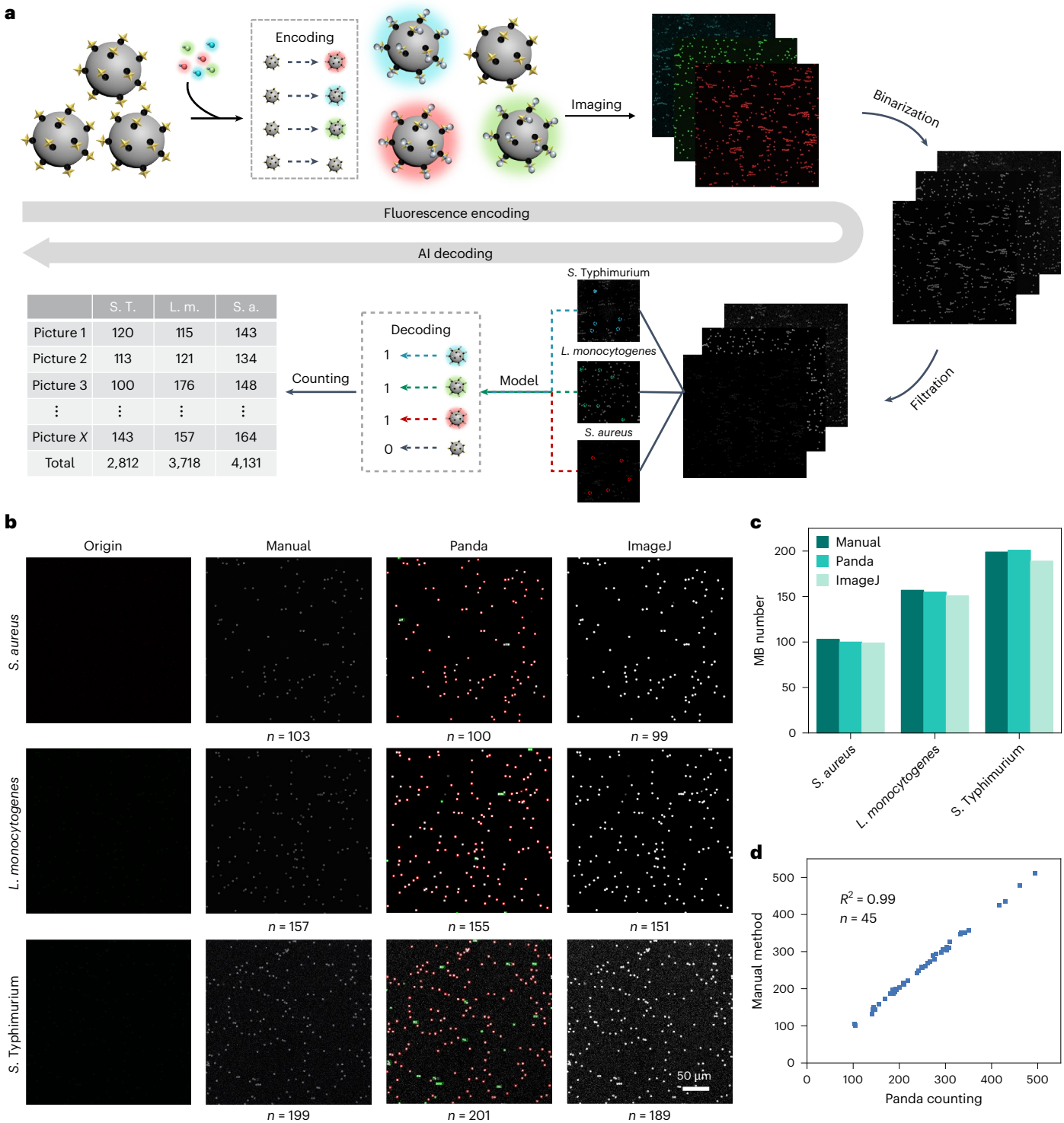


| | S. T. | L. m. | S. a. |
|---|---|---|---|
| Picture 1 | 120 | 115 | 143 |
| Picture 2 | 113 | 121 | 134 |
| Picture 3 | 100 | 176 | 148 |
| ⋮ | ⋮ | ⋮ | ⋮ |
| Picture *X* | 143 | 157 | 164 |
| Total | 2,812 | 3,718 | 4,131 |

**Fig. 3 | Programmable MB-assisted imaging transcoding system. a**, Process of fluorescent MB encoding and the Panda algorithm mediated the AI decoding for the obtained images. S. T., *S.* Typhimurium; L. m., *L. monocytogenes*; S. a. *S. aureus*. **b**, Statistical comparison of different software programs for counting fluorescent MB spheres in the images. The scale bar applies to all images in **b**. **c**, Number of fluorescent spheres according to different software programs. **d**, Consistency of the manual method and our Panda software.

by Panda were 201, 100 and 155 for *S.* Typhimurium, *S. aureus* and *L. monocytogenes*, respectively. These numbers showed good consistency with those of the manual method (Fig. 3b,d), with minor discrepancies potentially arising from subjective errors during operation. This manual method proved that Panda could effectively decode the encoded images. However, compared with Panda and the manual method, the commercial software ImageJ showed less consistency (Fig. 3b,c). This disparity could be attributed to the homogeneous processing nature of ImageJ and improper threshold adjustments, which hindered optimal readouts. Following the decoding process, standard curves were established to establish the association between food-borne pathogen DNA concentrations and the number of MB–TA–SA microspheres.

https://doi.org/10.1038/s43016-024-01082-y

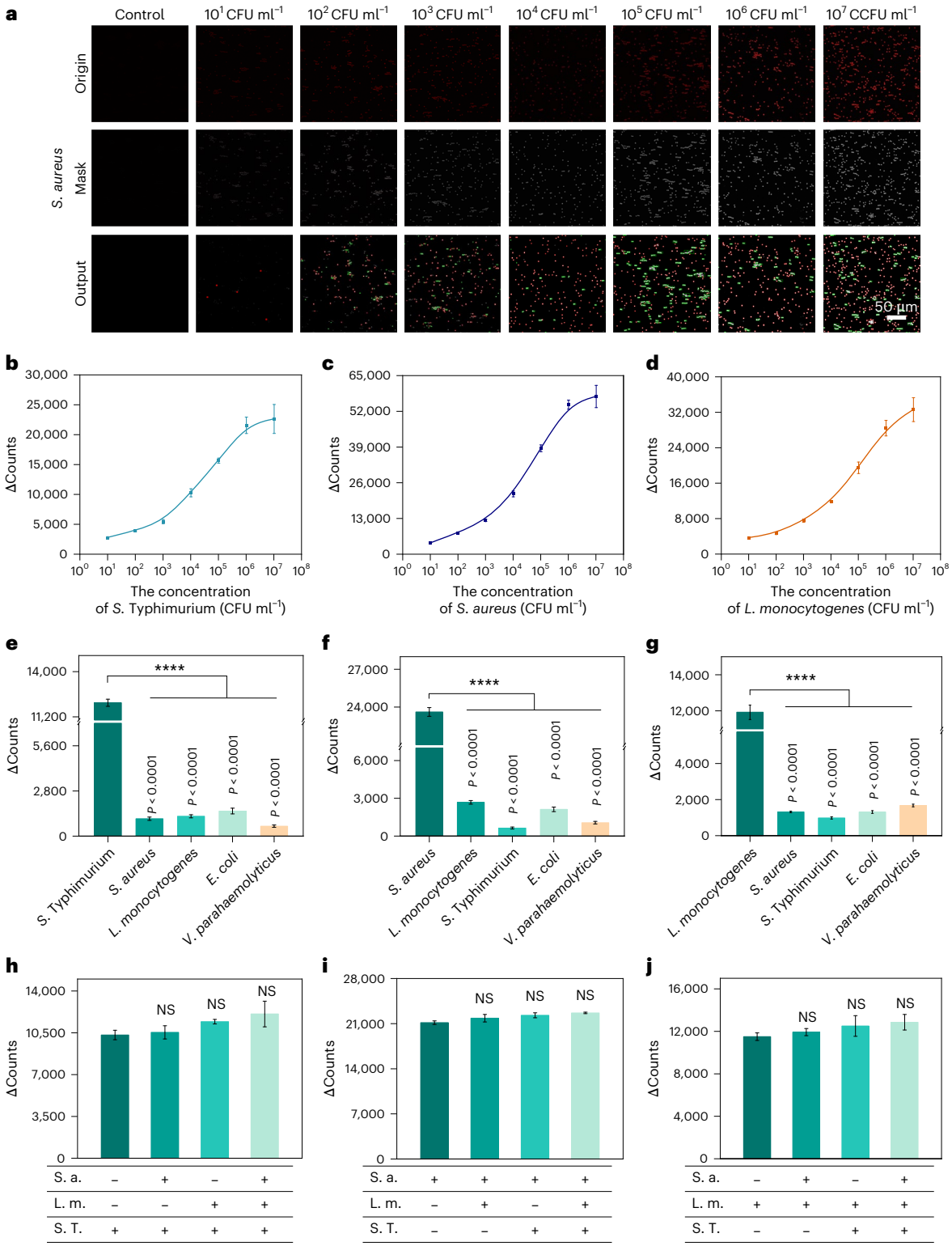


**Fig. 4 | Single food-borne pathogen detection using d-MAGIC. a**, Fluorescence map and its results as processed by Panda (origin: images obtained by CLSM; mask: original images processed via binarization; output: the images recognized after Panda; the experiments were repeated independently three times, and each concentration counted by 30 pictures, $n = 3$). The scale bar applies to all images in **a**. **b**–**d**, Relationship between different concentrations of food-borne pathogens, *S.* Typhimurium (**b**), *S. aureus* (**c**) and *L. monocytogenes* (**d**), and the signal processed by AI. **e**–**g**, d-MAGIC for the detection of the three food-borne pathogens, *S.* Typhimurium (**e**), *S. aureus* (**f**) and *L. monocytogenes* (**g**), under different types of interference. The concentration of non-target bacteria is 100-fold higher than that of target bacteria. Data are presented as means ± s.d., $n = 3$. *P* values were calculated using two-sided one-way ANOVA post-Dunnett's test; ****$P < 0.0001$. **h**–**j**, Specificity property of d-MAGIC: *S.* Typhimurium (**h**), *S. aureus* (**i**) and *L. monocytogenes* (**j**). Data are presented as means ± s.d., $n = 3$. *P* values were calculated using two-sided one-way ANOVA post-Dunnett's test. NS, non-significant.

https://doi.org/10.1038/s43016-024-01082-y

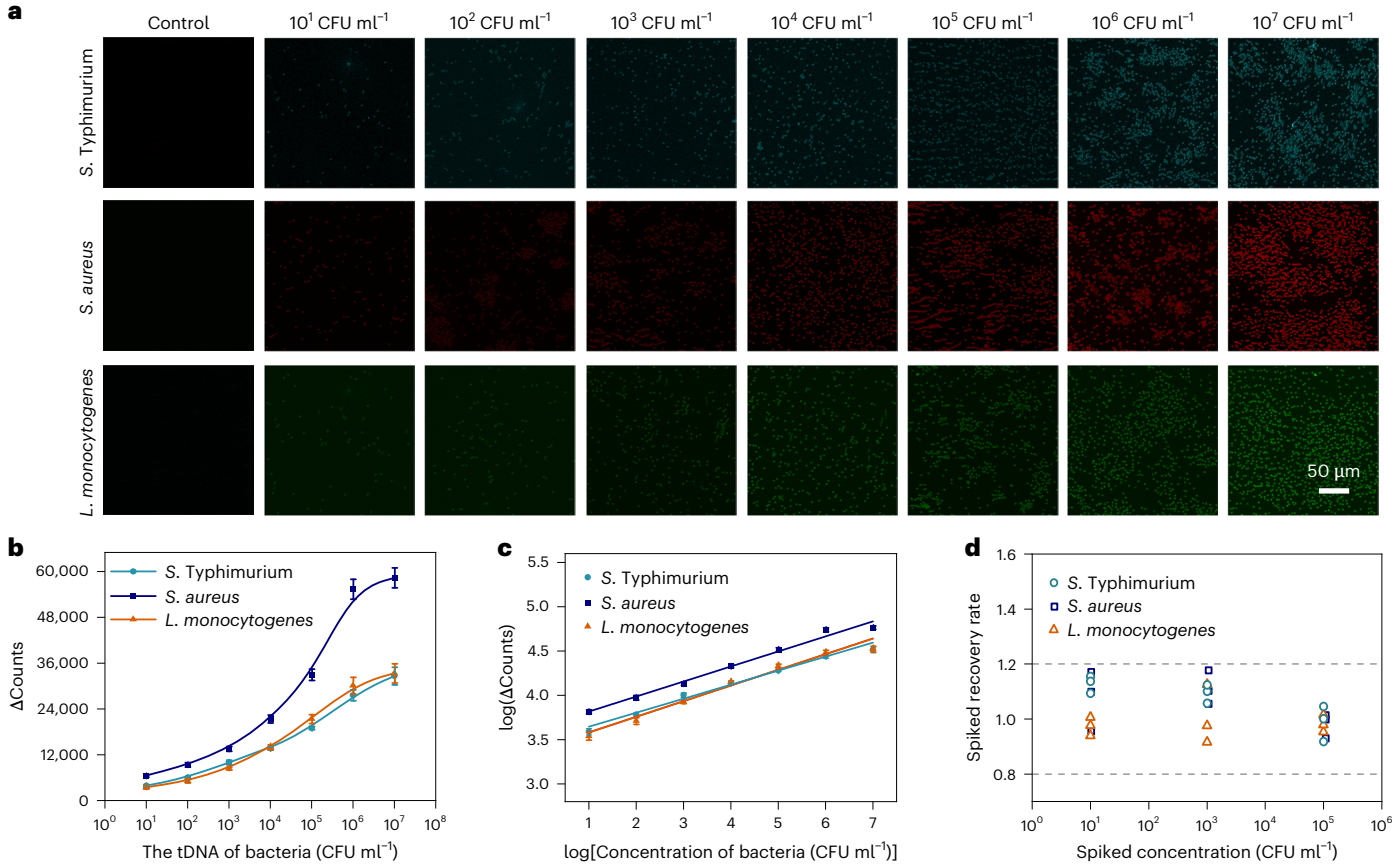


**Fig. 5 | Multiplexed detection of three food-borne pathogens. a**, Fluorescence images of three food-borne pathogens at different concentrations (the experiments were repeated independently three times and each concentration counted by 30 pictures, $n = 3$). The scale bar applies to all images in **a**. **b**, Relationship between different concentrations of food-borne pathogens and the signal processed by AI (the data are presented as means ± s.d., $n = 3$). **c**, Linear regression of multiple detections of the three food-borne pathogens (the data are presented as means ± s.d., $n = 3$). **d**, Recovery rate of d-MAGIC for the three food-borne pathogens spiked in samples at different concentrations (the dots refer to the recovery of bacterial DNA).

## Single food-borne pathogen detection

A study was conducted to investigate the sensitivity of the d-MAGIC method in detecting three strains of food-borne pathogens (*S.* Typhimurium, *S. aureus* and *L. monocytogenes*) under optimized parameters. The method used the specific gDNAs (Fig. 4a and Supplementary Fig. 5a,b) and fluorescence reporters of three food-borne pathogens to encode on MB–TA–SA conjugates (Fig. 3), which were decoded using AI. The d-MAGIC method successfully detected all three food-borne pathogens at lower concentrations ranging from $10^1$ CFU ml$^{-1}$ to $10^7$ CFU ml$^{-1}$ (Fig. 4b–d), consistent with traditional ddPCR. However, ddPCR showed a narrower range, detecting concentrations from $10^2$ CFU ml$^{-1}$ to $10^7$ CFU ml$^{-1}$ for *S.* Typhimurium and *L. monocytogenes*, and from $10^2$ CFU ml$^{-1}$ to $10^6$ CFU ml$^{-1}$ for *S. aureus* (Supplementary Fig. 6). This difference may be attributed to false-positive signals at low concentrations and signal saturation at high concentrations in ddPCR. The number of encoding MB–TA–SA conjugates was decoded by AI, showing an excellent linear association ($R^2 > 0.98$) between the concentration of the three bacteria and a limit of detection (LOD) of 7 CFU ml$^{-1}$ for *S.* Typhimurium, 6 CFU ml$^{-1}$ for *S. aureus* and 6 CFU ml$^{-1}$ for *L. monocytogenes* (Supplementary Fig. 5c–e). The high sensitivity of d-MAGIC can be attributed to the ultrasensitive digital signal readout strategy and the strong combination between biotin and streptavidin, allowing the concentration of single biotinylation fluorescent probes on the surface of MB–TA–SA conjugates, resulting in signal enrichment without amplification. This advantage is not available in conventional amplification methods as the fluorescence readout requires sufficient intensity to realize signal readout. These results show the potential of the d-MAGIC method for rapid and accurate detection of food-borne pathogens, with possible applications in bacterial detection requiring a simple design for specific gDNA.

TS: Please change 'Δ counts' to 'ΔCounts' in panel b.To ensure the specificity and minimize interference in d-MAGIC, the study investigated the signals produced by interfering with food-borne pathogen DNA. The signals were found to be lower than 13% of the target bacteria (Fig. 4e–g), which could be attributed to mismatches and the non-specific cleavage ability of CbAgo. However, these signals did not significantly impact the results. Therefore, the CbAgo cleavage reaction guided by two gDNAs shows excellent specificity for each species of food-borne pathogen when the gDNAs are specific (Fig. 4h–j). In addition, no cross-reactivity was observed between the gDNA for *S.* Typhimurium, *S. aureus* and *L. monocytogenes*; the DNA of the three food-borne pathogens triggered noticeable signal changes, ensuring the accuracy of the d-MAGIC method.

## Multiplexed detection of three food-borne pathogens

We conducted further investigation into the application of d-MAGIC for the multiplexed detection of food-borne pathogens. This was based on the excellent specific cleavage of CbAgo and its anti-interference properties. The results were satisfactory, showing that the sensitivity of d-MAGIC for multiplexed detection was

https://doi.org/10.1038/s43016-024-01082-y

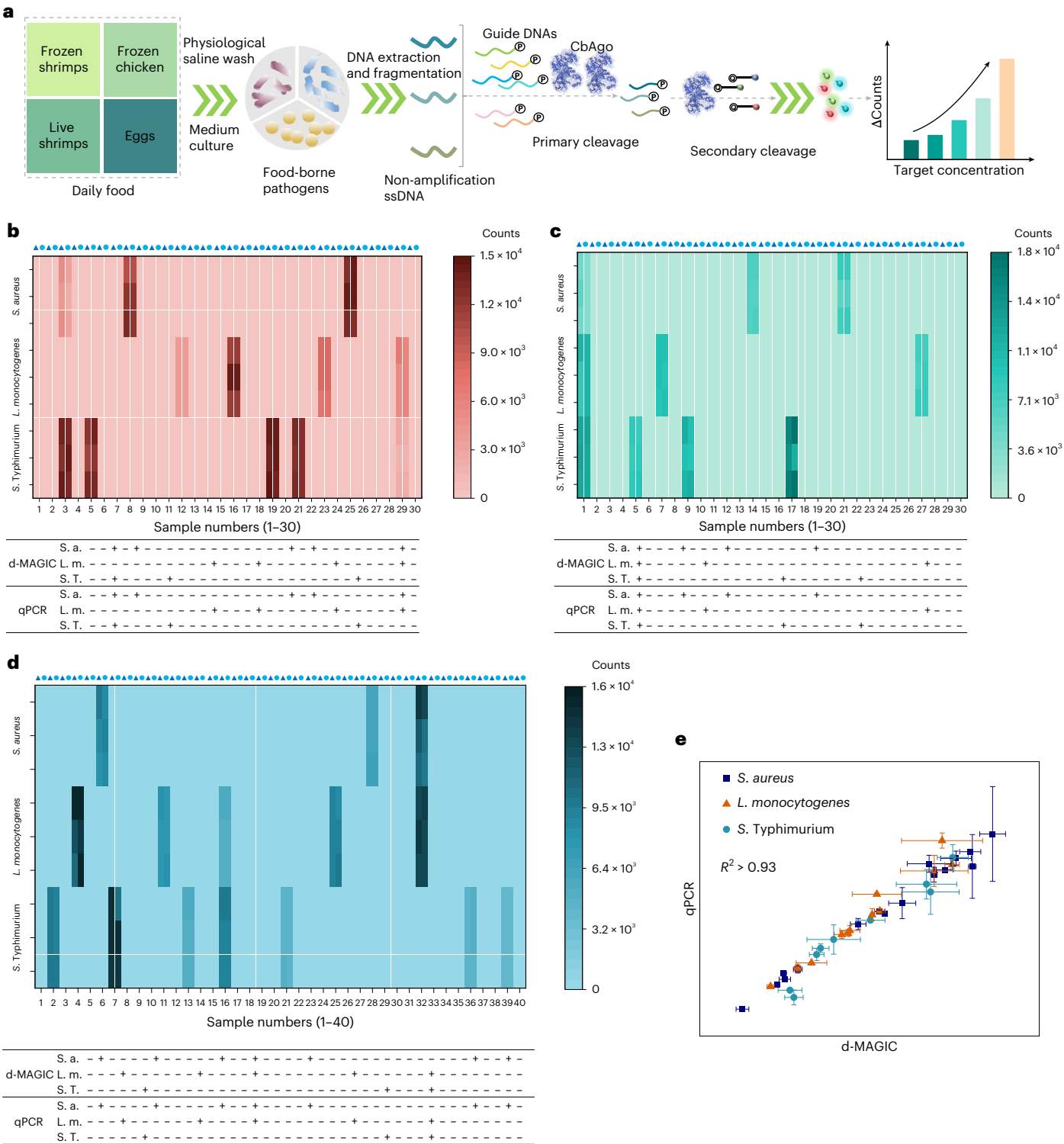


**Fig. 6 | Real sample analysis by d-MAGIC (triangle) and qPCR (circle) for detecting food-borne pathogens. a**, Illustration of detection procedures in real samples (PDB code 6QZK). **b**, Analysis of egg samples. **c**, Analysis of chicken samples. **d**, Analysis of live (numbers 1–20) and frozen (numbers 21–40) shrimp samples. **e**, Accuracy comparison between d-MAGIC and qPCR. The data represent the means ± s.d. of three replications ($n = 3$).

comparable to that of single bacteria detection, with a detection range from $10^1$ CFU ml$^{-1}$ to $10^7$ CFU ml$^{-1}$. Furthermore, the detection ability for the three bacteria remained consistent (Figs. 5a–c and Supplementary Fig. 7). To validate the multiplexed detection, recovery tests were performed by spiking three different concentrations of food-borne pathogens ($10^1$, $10^3$ and $10^5$ CFU ml$^{-1}$ for *S.* Typhimurium, *S. aureus* and *L. monocytogenes*, respectively) into actual non-detected samples. The average recovery rates (Fig. 5d) for *S.* Typhimurium, *S. aureus* and *L. monocytogenes* were between 91% and 113% (Supplementary Table 4), showing that d-MAGIC could achieve multiplexed detection and exhibited excellent performance even in complex samples. Furthermore, due to its digital

signal readout, d-MAGIC has better stability and anti-interference (reporter) than previous work[42] (Supplementary Fig. 8).

### Real sample analysis

To assess the applicability of d-MAGIC in detecting food-borne pathogens, we randomly selected 100 samples from a local store, including live shrimp, frozen shrimp, eggs and frozen chicken, for testing. We compared the results obtained from d-MAGIC and qPCR (Fig. 6a). Of the 100 samples, 16 were positive for *S.* Typhimurium, 9 were positive for *S. aureus* and 12 were positive for *L. monocytogenes* according to d-MAGIC (Fig. 6b–d). qPCR was used as a control method for detecting these real samples. The two methods showed good consistency, with a correlation coefficient greater than 0.93 for detecting the three pathogens (Fig. 6e). These results show that our d-MAGIC method exhibits excellent analytical performance and can accurately quantify food-borne pathogens in real food samples. We also compared d-MAGIC with other representative methods (Supplementary Table 5) for food-borne pathogen detection. The reported methods have some drawbacks, such as time consumption and the requirement for DNA amplification, which could not be avoided. Fortunately, d-MAGIC overcomes these limitations and allows fluorescence probe aggregation and signal enrichment, eliminating the need for complicated amplification processes and achieving high sensitivity in nucleic acid detection.

## Discussion

In contrast to traditional digital methods that rely on single droplets and microfluidics[43–45], our study adopted uniform MBs as the carrier instead of droplets for digitization. The MBs were labelled with fluorescence probes and decoded using our self-developed AI software (Panda). This innovative approach enables a digital nucleic acid test assay without the need for water-in-oil droplets or complex DNA amplification processes. Furthermore, the specific cleavage ability of CbAgo overcomes issues related to non-specific cleavage, giving the CbAgo-based sensor the capability for multiplexed detection[19,23]. Furthermore, unlike CRISPR–Cas, CbAgo proteins can cleave DNA and RNA in a sequence-specific manner, ensuring accurate and specific detection. The products resulting from the primary cleavage guided by two specific gDNAs can serve as a new guide for the secondary cleavage to cleave the FQ reporter[27,28] (Supplementary Fig. 9a,b).

Moreover, using MBs as the digital readout signal carrier eliminates background signal interference and the disadvantages of using water in oil, which is highly susceptible to environmental factors (Supplementary Fig. 9c). By using the biotin–streptavidin interaction, fluorescent molecules can be concentrated on the surface of the MB–TA–SA conjugate, enhancing the conjugation sites through tyramine amplification[46]. This approach enriches signal probes and enables low-concentration detection without the need for amplification. In addition, the ultra-high resolution of CLSM allows the detection of weak fluorescence signals, contributing to the amplification-free detection of food-borne pathogens. Finally, we integrated our self-developed Panda software to decode the fluorescence-encoded MBs, ensuring the accuracy and sensitivity of our method.

## Conclusion

We have developed a powerful and programmable method for digital nucleic acid detection called amplification-free MB-assisted imaging transcoding. This method enables the simultaneous detection of food-borne pathogens without the need for DNA amplification. It achieves this by combining an accurate CbAgo cleavage system with the MB–TA–SA conjugate encoding strategy. In addition, through the utilization of AI technology, we can effectively decode fluorescence-encoding MB conjugates, enabling digital, multiplexed, DNA-amplification-free detection of food-borne pathogens. This method has shown an extremely sensitive ability to detect multiple food-borne pathogens, outperforming other approaches (Supplementary Table 6). It also overcomes the limitations of traditional digital methods and offers a straightforward, fast, user-friendly approach that uses a single enzyme-mediated multiplexed strategy for digital nucleic acid detection. The potential applications of this approach extend to clinical nucleic acid detection, and we encourage researchers to capitalize on biotechnology to improve the efficiency of argonaute enzyme cleavage and develop portable devices for point-of-care testing.

## Methods

### Reagents

Carboxylic-acid-modified MBs with a diameter of 3 μm were purchased from Ocean NanoTech. *N*-hydroxysulfosuccinimide (NHS) and 1-ethyl-3-(3-dimethylaminopropyl) carbodiimide hydrochloride (EDC), hydrogen peroxide ($H_2O_2$), TRIS hydrochloride (Tris–HCl), manganous chloride ($MnCl_2$) and sulfuric acid ($H_2SO_4$) were procured from Sigma-Aldrich. The streptavidin, 3,3′,5,5′-tetramethylbenzidine (TMB) buffer and horseradish peroxidase (HRP) were obtained from Beyotime Biotechnology. Reagents such as TA were sourced from Sinopharm Chemical, and deionized water was produced using a microporous Milli-Q ion exchange device (Millipore). All 5-fluorescence-labelled oligonucleotides (FQ reporters) and 5-phosphorylated gDNA were purchased from Sangon Biotech. The ddPCR kit was purchased from Bio-Rad Laboratories.

### Fabrication of MB–TA–SA conjugates

To modify the MBs, we added 100 μl of NHS, EDC and the appropriate amount of tyramine to a 200 μl MB (10 mg $ml^{-1}$) suspension. The mixture was then shaken at room temperature for 12 h (refs. 46,47). Excess tyramine molecules were removed using magnetic separation, and the resulting product was washed three times with ultrapure water. After each wash, the modified MBs were isolated using magnetic separation. The washed products were then redissolved in 190 μl of ultrapure water and mixed with the appropriate amount of $H_2O_2$ and 200 μl of streptavidin. The mixture was further reacted with HRP (dilution 2,000 times) for 10 min to catalyse the formation of MB–TA–SA conjugates. After three additional washes with magnetic separation, the conjugates were redissolved in ultrapure water. The final volume was adjusted to 200 μl, and the product was stored at 4 °C until further use.

### d-MAGIC for single food-borne pathogen detection

Firstly, 2 μl of a 1 mg $ml^{-1}$ CbAgo solution and 2 μl of two specific gDNAs (G1 and G2) were mixed in a centrifuge tube. The gDNA concentration used was 3 μM for *S.* Typhimurium, 2 μM for *S. aureus* and 5 μM for *L. monocytogenes*. The mixture was then shaken on a vortex for 2 min. Next, 2 μl of each buffer (20 mM, pH = 7.5, Tris–HCl buffer and 2 μl 500 μM $MnCl_2$) was gently added to the prepared tube while continuously shaking. The mixture was incubated for 10 min at 37 °C. After the incubation, 2 μl of target DNA from the pathogenic bacteria was added to each tube and incubated for 20 min at 37 °C. Following this, 2 μl of fluorescence-labelled FQ reporters was added to each tube. The FQ reporter concentrations used were 2 μM for *S.* Typhimurium, 3 μM for *S. aureus* and 2 μM for *L. monocytogenes*. The tubes were then incubated for an additional 20 min. The resulting product was mixed with 50 μl of MB–TA–SA conjugates and rotated gently for 30 min to allow fluorescence encoding. Finally, the products were magnetically separated three times and brought to a final volume of 20 μl using nuclease-free water.

### Data acquisition of encoding MB–TA–SA conjugates and AI decoding

Confocal Petri dishes with biotin-modified FQ reporters incorporated into MB–TA–SA conjugates were used for fluorescence encoding. A mixture of 30 ml was added to the containers and sealed with

a 20 mm × 20 mm coverslip. CLSM was used to monitor the results of each sample using FV31S-SW software. Images were obtained under the variable bandwidth filter (VBF) mode with different emission absorbances (λem = 402 nm, λem = 492 nm, λem = 550 nm). A total of 30 pictures were captured for random areas at each concentration, with 3 independent replicates performed. The fluorescence images obtained were categorized by colour and decoded using software based on an AI algorithm named 'Panda'. To eliminate background interference, the images were converted into greyscale images through binarization and filtered. Statistical analysis of the MB–TA–SA–bio–FQ reporter conjugates was conducted by counting the remaining numbers of MBs in different categories after filtration. MBs with fluorescence intensity above the threshold were assigned a count of 1, whereas those below the threshold were assigned 0.

### d-MAGIC for multiplexed detection of three food-borne pathogens

The experimental procedure for single detection reactions was replicated for the multiplexed detection, with some modifications. Instead of using one food-borne pathogen in one tube, the gDNA, target DNA and FQ reporter of three types of food-borne pathogens were used simultaneously in a single reaction. The procedure was as follows: 2 µl of 1 mg $ml^{-1}$ CbAgo and 2 µl of two specific gDNAs (G1 and G2) (3 µM for *S.* Typhimurium, 2 µM for *S. aureus* and 5 µM for *L. monocytogenes*) for each food-borne pathogen were mixed in a centrifuge tube and shaken for 2 min on a vortex. Then, 2 µl of each buffer (20 mM pH = 7.5 Tris–HCl buffer and 2 µl 500 µM $MnCl_2$) was gently added to the prepared tube. The mixture was incubated for 10 min at 37 °C. Next, 2 µl of target DNA from each food-borne pathogen was added to each tube and incubated at 37 °C for 20 min. Subsequently, 2 µl of fluorescence-labelled FQ reporters (2 µM for *S.* Typhimurium, 3 µM for *S. aureus* and 2 µM for *L. monocytogenes*) for each food-borne pathogen was added to each tube and incubated for 20 min. The resulting product was then mixed with 50 µl of MB–TA–SA conjugates and rotated gently for 30 min for fluorescence encoding. Finally, the products were magnetically separated three times and brought to a final volume of 30 µl with nuclease-free water. The LOD was calculated using the equation LOD = 3*S*/*M*, where *S* is the standard deviation of blank samples and *M* is the slope of the standard curve at a low concentration range.

### Specificity and anti-interference capability

To evaluate the specificity of the gDNA and FQ reporters used in the experiment, five distinct food-borne pathogens (*S.* Typhimurium, *S. aureus*, *L. monocytogenes*, *Escherichia coli* and *Vibrio parahaemolyticus*) were selected. These pathogens were reacted with MB–TA–SA conjugates and the accurate CbAgo cleavage system, and the concentration of the sample pathogens was $10^4$ CFU $ml^{-1}$, whereas the concentration of the interference pathogens was $10^6$ CFU $ml^{-1}$. The specificity and sequence operation steps for the detection were consistent with those used for single bacteria detection. The fluorescent signals produced by the accurate CbAgo cleavage system, encoding to the MB–TA–SA conjugates, were detected by CLSM and decoded using the 'Panda' software based on an AI algorithm.

Furthermore, to evaluate the assay's anti-interference ability, we performed a reaction using the same bacterial gDNA and fluorescent probe for one food-borne pathogen. However, the substrates used were a mixture of different bacterial DNAs used in the multiplexed detection. Specifically, we selected gDNA and FQ reporters for *S. aureus*, and the substrates used in this reaction consisted of a mixture of *S. aureus*, *S. aureus* with *L. monocytogenes*, *S. aureus* with *S.* Typhimurium, *S. aureus* with a mixture of *L. monocytogenes* and *S.* Typhimurium, and ultrapure water. The number of encoded MB–TA–SA conjugates that showed a fluorescent signal under CLSM was determined using the 'Panda' software, which uses an AI algorithm for decoding.

### Recovery and real sample analysis

To assess our method's applicability in real-life scenarios, we randomly selected 100 samples, including live shrimp, frozen shrimp, eggs and frozen chicken, from a local store. To collect bacterial DNA, each sample was immersed in 50 ml of physiological saline for 30 min. We then took 2 ml of the washing solution to incubate potential food-borne pathogens in a tryptic soybean peptone liquid medium for 6 h. The egg samples were processed by washing the eggshells, following the same procedure used with the other samples. DNA was extracted from 3 ml of each medium using a bacterial genomic DNA extraction kit (B518225-0050, Sangon Biotech, produced by Omega), and the extracted DNA was heated at 98 °C for 15 min to obtain single-stranded DNA (ssDNA), which was then quickly cooled at −20 °C for 20 min. The obtained ssDNA was stored at −20 °C. The testing followed the same steps as single bacteria detection, except that the extracted DNA from actual samples was used as the target DNA. In addition, three non-detected samples were spiked with $10^1$ CFU $ml^{-1}$, $10^3$ CFU $ml^{-1}$ and $10^5$ CFU $ml^{-1}$ of food-borne pathogen target DNA to calculate recovery.

### Reporting summary

Further information on research design is available in the Nature Portfolio Reporting Summary linked to this article.

## Data availability

Source data are provided with this paper.

## Code availability

The related code is available via GitHub at https://github.com/Wang-Qinyu/Panda/tree/main.

## References

1. *Food Safety* (World Health Organization, 2023); https://www.who.int/health-topics/food-safety#tab=tab_1
2. Vikram, A., Callahan, M. T., Woolston, J. W., Sharma, M. & Sulakvelidze, A. Phage biocontrol for reducing bacterial foodborne pathogens in produce and other foods. *Curr. Opin. Biotechnol.* **78**, 102805 (2022).
3. Tavelli, R., Callens, M., Grootaert, C., Abdallah, M. F. & Rajkovic, A. Foodborne pathogens in the plastisphere: can microplastics in the food chain threaten microbial food safety? *Trends Food Sci. Technol.* **129**, 1–10 (2022).
4. Lee, H.-W. et al. Identification of microbial communities, with a focus on foodborne pathogens, during kimchi manufacturing process using culture-independent and -dependent analyses. *LWT Food Sci. Technol.* **81**, 153–159 (2017).
5. Wei, C. et al. Recent progress on lateral flow immunoassays in foodborne pathogen detection. *Food Biosci.* **52**, 102475 (2023).
6. Rantsiou, K. & Cocolin, L. in *Advances in Microbial Food Safety* (ed. Sofos, J.) Ch. 10 (Woodhead Publishing, 2013).
7. Lee, S. Y., Kim, J. H. & Oh, S. W. Combination of filtration and immunomagnetic separation based on real-time PCR to detect foodborne pathogens in fresh-cut apple. *J. Microbiol. Methods* **201**, 106577 (2022).
8. Aslanzadeh, J. Preventing PCR amplification carryover contamination in a clinical laboratory. *Ann. Clin. Lab. Sci.* **34**, 389–396 (2004).
9. Borst, A., Box, A. T. A. & Fluit, A. C. False-positive results and contamination in nucleic acid amplification assays: suggestions for a prevent and destroy strategy. *Eur. J. Clin. Microbiol. Infect. Dis.* **23**, 289–299 (2004).
10. Rutty, G. N., Hopwood, A. & Tucker, V. The effectiveness of protective clothing in the reduction of potential DNA contamination of the scene of crime. *Int. J. Legal Med.* **117**, 170–174 (2003).

11. Morono, Y. et al. Assessment of capacity to capture DNA aerosols by clean filters for molecular biology experiments. *Microbes Environ.* **33**, 222–226 (2018).
12. Wu, H. et al. DropCRISPR: a LAMP-Cas12a based digital method for ultrasensitive detection of nucleic acid. *Biosens. Bioelectron.* **211**, 114377 (2022).
13. Wu, X. et al. Digital CRISPR-based method for the rapid detection and absolute quantification of nucleic acids. *Biomaterials* **274**, 120876 (2021).
14. Ali, Z., Mahas, A. & Mahfouz, M. CRISPR/Cas13 as a tool for RNA interference. *Trends Plant Sci.* **23**, 374–378 (2018).
15. Kaminski, M. M., Abudayyeh, O. O., Gootenberg, J. S., Zhang, F. & Collins, J. J. CRISPR-based diagnostics. *Nat. Med.* **24**, 702 (2018).
16. Xing, G. et al. Multiplexed detection of foodborne pathogens using one-pot CRISPR/Cas12a combined with recombinase aided amplification on a finger-actuated microfluidic biosensor. *Biosens. Bioelectron.* **220**, 114885 (2023).
17. Leung, R. K. et al. CRISPR–Cas12-based nucleic acids detection systems. *Methods* **203**, 276–281 (2022).
18. Chen, L., Ding, J., Yuan, H., Chen, C. & Li, Z. Deep-dLAMP: deep learning-enabled polydisperse emulsion-based digital loop-mediated isothermal amplification. *Adv. Sci.* **9**, e2105450 (2022).
19. Xun, G. et al. Argonaute with stepwise endonuclease activity promotes specific and multiplex nucleic acid detection. *Bioresour. Bioprocess* **8**, 46 (2021).
20. Kuzmenko, A. et al. DNA targeting and interference by a bacterial Argonaute nuclease. *Nature* **587**, 632–637 (2020).
21. Yang, L. et al. *Pyrococcus furiosus* Argonaute combined with recombinase polymerase amplification for rapid and sensitive detection of *Enterocytozoon hepatopenaei*. *J. Agric. Food Chem.* **71**, 944–951 (2023).
22. Liu, Q. et al. Argonaute integrated single-tube PCR system enables supersensitive detection of rare mutations. *Nucleic Acids Res.* **49**, e75 (2021).
23. Ye, X. et al. Argonaute-integrated isothermal amplification for rapid, portable, multiplex detection of SARS-CoV-2 and influenza viruses. *Biosens. Bioelectron.* **207**, 114169 (2022).
24. Song, J. et al. Highly specific enrichment of rare nucleic acid fractions using *Thermus thermophilus* Argonaute with applications in cancer diagnostics. *Nucleic Acids Res.* **48**, e19 (2020).
25. Wang, Y. et al. In vitro Argonaute cleavage-mediated quantitative PCR facilitates versatile CRISPR/Cas-induced mutant analysis. *Sens. Actuators B* **374**, 132781 (2023).
26. Kuzmenko, A., Yudin, D., Ryazansky, S., Kulbachinskiy, A. & Aravin, A. A. Programmable DNA cleavage by Ago nucleases from mesophilic bacteria *Clostridium butyricum* and *Limnothrix rosea*. *Nucleic Acids Res.* **47**, 5822–5836 (2019).
27. Vaiskunaite, R., Vainauskas, J., Morris, J. J. L., Potapov, V. & Bitinaite, J. Programmable cleavage of linear double-stranded DNA by combined action of Argonaute CbAgo from *Clostridium butyricum* and nuclease deficient RecBC helicase from *E. coli*. *Nucleic Acids Res.* **50**, 4616–4629 (2022).
28. Hegge, J. W. et al. DNA-guided DNA cleavage at moderate temperatures by *Clostridium butyricum* Argonaute. *Nucleic Acids Res.* **47**, 5809–5821 (2019).
29. Wang, Z. et al. Mesophilic Argonaute-mediated polydisperse droplet biosensor for amplification-free, one-pot, and multiplexed nucleic acid detection using deep learning. *Anal. Chem.* **96**, 2068–2077 (2024).
30. Hafiz, M. et al. Magnetic nanoparticles draw solution for forward osmosis: current status and future challenges in wastewater treatment. *J. Environ. Chem. Eng.* **10**, 108955 (2022).
31. Chavan, N., Dharmaraj, D., Sarap, S. & Surve, C. Magnetic nanoparticles—a new era innanotechnology. *J. Drug Deliv. Sci. Technol.* **77**, 103899 (2022).
32. Binandeh, M. Performance of unique magnetic nanoparticles in biomedicine. *Eur. J. Med. Chem. Rep.* **6**, 100072 (2022).
33. Fu, C. et al. Horseradish peroxidase-repeat assay based on tyramine signal amplification for highly sensitive $H_2O_2$ detection by surface-enhanced Raman scattering. *Analyst* **146**, 7320–7326 (2021).
34. Chen, Q. et al. A highly-sensitive colorimetric assay method for antibody array based on an tyramide signal amplification system. *Anal. Lett.* **45**, 219–226 (2012).
35. Gombolay, G. Y. et al. Review of machine learning and artificial intelligence (ML/AI) for the pediatric neurologist. *Pediatr. Neurol.* **141**, 42–51 (2023).
36. Moon, G. et al. Machine learning-based design of meta-plasmonic biosensors with negative index metamaterials. *Biosens. Bioelectron.* **164**, 112335 (2020).
37. Wang, S. K. et al. Single-cell multiome of the human retina and deep learning nominate causal variants in complex eye diseases. *Cell Genom.* **2**, 100164 (2022).
38. Long, E. et al. The case for increasing diversity in tissue-based functional genomics datasets to understand human disease susceptibility. *Nat. Commun.* **13**, 2907 (2022).
39. Shameer, K., Tripathi, L. P., Kalari, K. R., Dudley, J. T. & Sowdhamini, R. Interpreting functional effects of coding variants: challenges in proteome-scale prediction, annotation and assessment. *Brief Bioinform.* **17**, 841–862 (2016).
40. Zander, A. et al. Guide-independent DNA cleavage by archaeal Argonaute from *Methanocaldococcus jannaschii*. *Nat. Microbiol.* **2**, 17034 (2017).
41. Swarts, D. C. et al. Autonomous generation and loading of DNA guides by bacterial Argonaute. *Mol. Cell* **65**, 985–998.e6 (2017).
42. Zhao, J. et al. A machine vision-assisted Argonaute-mediated fluorescence biosensor for the detection of viable *Salmonella* in food without convoluted DNA extraction and amplification procedures. *J. Hazard. Mater.* **466**, 133648 (2024).
43. Hou, Y., Chen, S., Zheng, Y., Zheng, X. & Lin, J.-M. Droplet-based digital PCR (ddPCR) and its applications. *Trac. Trends Anal. Chem.* **158**, 116897 (2023).
44. Cretich, M., Daaboul, G. G., Sola, L., Unlu, M. S. & Chiari, M. Digital detection of biomarkers assisted by nanoparticles: application to diagnostics. *Trends Biotechnol.* **33**, 343–351 (2015).
45. Xiang, X., Shang, Y., Zhang, J., Ding, Y. & Wu, Q. Advances in improvement strategies of digital nucleic acid amplification for pathogen detection. *Trac. Trends Anal. Chem.* **149**, 116568 (2022).
46. von Wasielewski, R. et al. Tyramine amplification technique in routine immunohistochemistry. *J. Histochem. Cytochem.* **45**, 1455–1459 (1997).
47. Stack, E. C., Wang, C., Roman, K. A. & Hoyt, C. C. Multiplexed immunohistochemistry, imaging, and quantitation: a review, with an assessment of tyramide signal amplification, multispectral imaging and multiplex analysis. *Methods* **70**, 46–58 (2014).


## Acknowledgements

We thank the National Natural Science Foundation of China (32172293), the National Key Research and Development Program of China (2022YFF0607900) and the Open Project of Key Laboratory of Detection Technology of Focus Chemical Hazards in Animal-Derived Food for State Market Regulation (number KF-202201) for financial support.

## Author contributions

Z.W. and Y.C. conceptualized the research. Z.W. and X.C. planned and performed the research. Z.W. assisted in testing the code. Z.W.

analysed the data. Z.W. wrote the original draft. A.M., F.J. and Y.C. reviewed and edited the paper.

## Competing interests
The authors declare no competing interests.

## Additional information
**Supplementary information** The online version contains supplementary material available at https://doi.org/10.1038/s43016-024-01082-y.

**Correspondence and requests for materials** should be addressed to Yiping Chen.

**Peer review information** *Nature Food* thanks Seyed Mohammad Taghi Gharibzahedi, Sang-Soon Kim and Fengge Song for their contribution to the peer review of this work.

nature portfolio

Corresponding author(s): Yiping Chen

Last updated by author(s): Oct 23, 2024

# Reporting Summary

Nature Portfolio wishes to improve the reproducibility of the work that we publish. This form provides structure for consistency and transparency in reporting. For further information on Nature Portfolio policies, see our Editorial Policies and the Editorial Policy Checklist.

## Statistics

For all statistical analyses, confirm that the following items are present in the figure legend, table legend, main text, or Methods section.

| n/a | Confirmed | |
|---|---|---|
| ☐ | ☒ | The exact sample size (*n*) for each experimental group/condition, given as a discrete number and unit of measurement |
| ☐ | ☒ | A statement on whether measurements were taken from distinct samples or whether the same sample was measured repeatedly |
| ☐ | ☒ | The statistical test(s) used AND whether they are one- or two-sided<br>*Only common tests should be described solely by name; describe more complex techniques in the Methods section.* |
| ☒ | ☐ | A description of all covariates tested |
| ☒ | ☐ | A description of any assumptions or corrections, such as tests of normality and adjustment for multiple comparisons |
| ☐ | ☒ | A full description of the statistical parameters including central tendency (e.g. means) or other basic estimates (e.g. regression coefficient) AND variation (e.g. standard deviation) or associated estimates of uncertainty (e.g. confidence intervals) |
| ☐ | ☒ | For null hypothesis testing, the test statistic (e.g. *F*, *t*, *r*) with confidence intervals, effect sizes, degrees of freedom and *P* value noted<br>*Give P values as exact values whenever suitable.* |
| ☒ | ☐ | For Bayesian analysis, information on the choice of priors and Markov chain Monte Carlo settings |
| ☒ | ☐ | For hierarchical and complex designs, identification of the appropriate level for tests and full reporting of outcomes |
| ☒ | ☐ | Estimates of effect sizes (e.g. Cohen's *d*, Pearson's *r*), indicating how they were calculated |

*Our web collection on statistics for biologists contains articles on many of the points above.*

## Software and code

Policy information about availability of computer code

| | |
|---|---|
| Data collection | The pictures were observed by the confocal laser scanning microscope imaging system (FV 3000) and captured by FLUOVIEW FV31S-SW. The digital droplet PCR was carried out by QX200. The Image J was used to count the magnetic beads in the pictures for comparison. The Circular dichroism was used to characterize the secondary structure. The scanning electron microscope was used to observe the morphology and element analysis. The nano particle potential analyzer was used to collect the zeta potential and particle size information. The computer code are available at https://github.com/Wang-Qinyu/Panda/tree/main. |
| Data analysis | The data was analyzed and drawn by Microsoft Excel and Origin Pro 2021. The line diagrams were drawn by Origin Pro 2021 (64-bit), © 1991-2020 Origin Lab Corporation. The scheme and figures was drawn and composed by Microsoft PowerPoint 2016, © Microsoft. The custom code was written in Python 3.6. |

For manuscripts utilizing custom algorithms or software that are central to the research but not yet described in published literature, software must be made available to editors and reviewers. We strongly encourage code deposition in a community repository (e.g. GitHub). See the Nature Portfolio guidelines for submitting code & software for further information.

## Data

Policy information about availability of data

All manuscripts must include a data availability statement. This statement should provide the following information, where applicable:

- Accession codes, unique identifiers, or web links for publicly available datasets
- A description of any restrictions on data availability
- For clinical datasets or third party data, please ensure that the statement adheres to our policy

Source data of the figures in main text are provided with this paper. The computer code are available at https://github.com/Wang-Qinyu/Panda/tree/main

## Research involving human participants, their data, or biological material

Policy information about studies with human participants or human data. See also policy information about sex, gender (identity/presentation), and sexual orientation and race, ethnicity and racism.

| | |
|---|---|
| Reporting on sex and gender | N/A |
| Reporting on race, ethnicity, or other socially relevant groupings | N/A |
| Population characteristics | N/A |
| Recruitment | N/A |
| Ethics oversight | N/A |

Note that full information on the approval of the study protocol must also be provided in the manuscript.

# Field-specific reporting

Please select the one below that is the best fit for your research. If you are not sure, read the appropriate sections before making your selection.

☒ Life sciences ☐ Behavioural & social sciences ☐ Ecological, evolutionary & environmental sciences

For a reference copy of the document with all sections, see nature.com/documents/nr-reporting-summary-flat.pdf

# Life sciences study design

All studies must disclose on these points even when the disclosure is negative.

| | |
|---|---|
| Sample size | The authors declare that no sample-size calculation was performed in this study. No sample size calculation was performed. For in vitro biochemical studies, three independent experiments were widely accepted and used in published paper (such as Nat Chem Biol. 17(4):387-393. doi: 10.1038/s41589-020- 00721.2). |
| Data exclusions | The authors declare that no data were excluded when analyzing because all obtained data were workable and rational. |
| Replication | The authors declare that the experiments were performed independently for at least three times. All attempts at replication were successful. |
| Randomization | The authors declare that the samples were allocated into experimental groups randomly in real sample analysis. |
| Blinding | The authors declare that no data were blinded to group allocation during data collection and/or analysis because all the data were workable and rational. And group allocation is not used. |

# Reporting for specific materials, systems and methods

We require information from authors about some types of materials, experimental systems and methods used in many studies. Here, indicate whether each material, system or method listed is relevant to your study. If you are not sure if a list item applies to your research, read the appropriate section before selecting a response.

## Materials & experimental systems

| n/a | Involved in the study |
|---|---|
| ☐ | ☒ Antibodies |
| ☒ | ☐ Eukaryotic cell lines |
| ☒ | ☐ Palaeontology and archaeology |
| ☒ | ☐ Animals and other organisms |
| ☒ | ☐ Clinical data |
| ☒ | ☐ Dual use research of concern |
| ☒ | ☐ Plants |

## Methods

| n/a | Involved in the study |
|---|---|
| ☒ | ☐ ChIP-seq |
| ☒ | ☐ Flow cytometry |
| ☒ | ☐ MRI-based neuroimaging |

# Antibodies

Antibodies used: primary antibody anti-His (Abbkine, ABT2050) at a dilution of 1:2500 and secondary antibody goat anti-mouse IgG (Kingsley) at a dilution of 1:10,000, with each change of incubation solution.

Validation: primary antibody anti-His (Abbkine, ABT2050) was used for detecting His-tag fusion of the expression CbAgo proteins. and the secondary antibody goat anti-mouse IgG (Kingsley) was used to bind to the expression CbAgo proteins labeled with primary antibodies to enhance detection signals for visual analysis.

# Plants

Seed stocks: The authors declare that no seed stocks or other plant material been used in this research.

Novel plant genotypes: The authors declare that no plant material been used in this research, so there is no novel plant genotypes to report.

Authentication: The authors declare that no seed stocks and novel plant genotypes found in this research, so there is no authentication to describe.